Morphology and Aggregation of RADA-16-I Peptide Studied by AFM, NMR and Molecular Dynamics Simulations

Dmitry Bagrov,[1,2] Yuliya Gazizova,[1,3] Victor Podgorsky,[1] Igor Udovichenko,[4,5] Alexey Danilkovich,[4,5] Kirill Prusakov,[1] Dmitry Klinov[1,6]

[1]*Scientific Research Institute of Physical–Chemical Medicine, Malaya Pirogovskaya, 1a Moscow 119435, Russian Federation*

[2]*Faculty of Biology, Department of Bioengineering, M.V. Lomonosov Moscow State University, Leninskie Gory, 1/73, Moscow 111991, Russian Federation*

[3]*Department of Biological and Medical Physics, Moscow Institute of Physics and Technology, Institutsky Lane 9, Dolgoprudny, Moscow Region 141700, Russian Federation*

[4]*Branch of Shemyakin and Ovchinnikov Institute of Bioorganic Chemistry, Russian Academy of Sciences, Prospect Nauki-6, Pushchino 142290, Russian Federation*

[5]*Pushchino State Institute of Natural Science, Prospect Nauki-3, Pushchino 142290, Russian Federation*

[6]*Shemyakin and Ovchinnikov Institute of Bioorganic Chemistry, Russian Academy of Sciences, Miklukho-Maklaya, 16/10, Moscow 117997, Russian Federation*

Received 7 April 2015; revised 31 August 2015; accepted 17 October 2015
Published online 26 October 2015 in Wiley Online Library (wileyonlinelibrary.com). DOI 10.1002/bip.22755

ABSTRACT:

RADA-16-I is a self-assembling peptide which forms biocompatible fibrils and hydrogels. We used molecular dynamics simulations, atomic-force microscopy, NMR spectroscopy, and thioflavin T binding assay to examine size, structure, and morphology of RADA-16-I aggregates. We used the native form of RADA-16-I (H-(ArgAlaAspAla)$_4$-OH) rather than the acetylated one commonly used in the previous studies. At neutral pH, RADA-16-I is mainly in the fibrillar form, the fibrils consist of an even number of stacked β-sheets. At acidic pH, RADA-16-I fibrils disassemble into monomers, which form an amorphous monolayer on graphite and monolayer lamellae on mica. RADA-16-I fibrils were compared with the fibrils of a similar peptide RLDL-16-I. Thickness of β-sheets measured by AFM was in excellent agreement with the molecular dynamics simulations. A pair of RLDL-16-I β-sheets was thicker (2.3 ± 0.4 nm) than a pair of RADA-16-I β-sheets (1.9 ± 0.1 nm) due to the volume difference between alanine and leucine residues. © *2015 Wiley Periodicals, Inc. Biopolymers (Pept Sci) 106: 72–81, 2016.*

Keywords: amyloid-like fibrils; atomic-force microscopy; RADA-16-I peptide; peptide monolayer; nuclear magnetic resonance

This article was originally published online as an accepted preprint. The "Published Online" date corresponds to the preprint version. You can request a copy of any preprints from the past two calendar years by emailing the Biopolymers editorial office at biopolymers@wiley.com.

Additional Supporting Information may be found in the online version of this article.

Correspondence to: Dmitry Bagrov, Scientific Research Institute of Physical–Chemical Medicine, Malaya Pirogovskaya, 1a, Moscow 119435, Russian Federation; e-mail: dbagrov@gmail.com

Contract grant sponsor: Russian Scientific Foundation
Contract grant number: 14-14-01001

© 2015 Wiley Periodicals, Inc.

INTRODUCTION

Amyloidosis is a term for a group of incurable diseases commonly associated with protein misfolding, with the best-known examples being Alzheimer's and Parkinson's diseases. A great effort is spent on understanding their biochemical basis and finding effective

therapies. From the molecular point, each type of amyloidosis is accompanied by the formation of amyloid fibrils.[1–3] Typically, they are linear, ~10 nm diameter fibrils made of peptides or proteins. They are insoluble *in vivo*, have a cross-β-spine backbone[4] and are able to bind to amyloid-specific dyes (Congo red and Thioflavin T). These features are remarkably insensitive to the amino-acid sequence and composition. If certain fibrils exhibit only some of these features, they are called amyloid-like, rather than amyloid.

Peptides consisting of alternating polar (hydrophylic) and nonpolar (hydrophobic) amino acids form amyloid-like fibrils made of β-sheets.[5] The aggregation of β-sheets exposes the polar residues to water and keeps the nonpolar ones inside the fibril. Surprisingly, artificial media based on peptide fibrils form a friendly environment for mammalian cells,[6] e.g., they can stimulate neuron growth *in vivo*[7] and function as a drug depot.[8]

RADA-16-I is one of the most widely discussed self-assembling peptides, which form amyloid-like fibrils. Hydrogels made of RADA-16-I can be used for various biomedical applications,[6] including hemostasis (bleeding prevention[9]) and regeneration of neurons.[10] In the field of tissue engineering the peptide sequence can be modified with short functional motifs to improve cell adhesion and differentiation.[11,12]

RADA-16-I has a very strong tendency to aggregation, thus RADA-16-I fibrils are very stable. Previous studies have shown that RADA-16-I forms amyloid-like nanofibrils which can be disassembled by sonication,[13] heating,[14] or pH change.[15] The aggregation of RADA-16-I (and similar RLDL-16-I) molecules is believed to occur through the four molecule cluster stage.[16,17] The cluster is stabilized by hydrogen bonds and the hydrophobic interaction between alanine residues.

The acetylated form of RADA-16-I is commonly used in the experimental studies.[9,13–15,18,19] Here we studied the structure and morphology of the normal peptide H-(ArgAlaAspAla)$_4$-OH with the native end groups. We tried to answer the following questions: what is an elementary building block of a mature fibril? How could we use the size measurements to answer this question? Is it possible to make RADA-16-I form a stable β-sheet monolayer?

To answer these questions, we examined the morphology and structure of RADA-16-I fibrils by AFM, NMR, and thioflavin T binding assay. We have shown that the fibrils consist of an even number of β-sheets (each fibril is a stack of bilayers, rather than monolayers). We compared RADA-16-I fibrils with the fibrils of a less investigated RLDL-16-I peptide,[16] having a similar sequence of alternating polar and non-polar residues. Fibril dissolution at low pH was studied by AFM and NMR. We have found that under certain experimental conditions RADA-16-I forms surface-induced lamellae which were interpreted as β-sheet monolayers.

EXPERIMENTAL SECTION

Reagents

Boc-L-amino acids and methylbenzhydrylamine resin hydrochloride (MBHA, 0.42 mmol g^{-1}) were obtained from the Peptide Institute (Osaka, Japan). Other reagents for peptide synthesis were obtained from IRIS Biotech Gmbh (Germany) and Fluka (Switzerland).

Solid-phase Peptide Synthesis

H-(ArgAlaAspAla)$_4$-OH (RADA-16-I) and H-(ArgLeuAspLeu)$_4$-OH (RLDL-16-I) peptides were synthesized according to the manual stepwise solid-phase synthesis protocol. All operations were carried out with occasional shaking. Solvent and reagent volumes used for the SPS operation corresponded to about 5 mL/0.5 g of starting MBHA resin. Those amounts were gradually increased to minimize the effects of peptide resin gradual swelling resulted from synthesized material accumulation.[20] Unconditional double coupling Boc-SPPS protocols were repeated 16 times, while the 1st coupling lasted for 3 h and the 2nd coupling was incubated overnight. Couplings were performed with three equivalents of Boc-amino acids activated with TBTU-NMM-HOBt.[21] Particular Boc-derivatives of Arg(Tos) and Asp(OcHx) were used. The coupling reaction completeness was probed at the 2nd coupling step with the qualitative ninhydrin-test.[22] The assembled polymer-bound 16-mers were washed with DCM, dried in vacuum to yield 922 mg of H-[Arg(Tos)-Ala-Asp(OcHx)-Ala]$_4$-MBHA and 930 mg of H-[Arg(Tos)-Leu-Asp(OcHx)-Leu]$_4$-MBHA resins. Peptide resins were subjected to the high HF cleavage procedure carried out with 15 mL of HF and 1 mL of m-cresol for 3 h at 0°C. At last, 390 mg of lyophilized crude peptide RADA-16-I and 360 mg of RLDL-16-I were obtained. Semi-preparative HPLC of 50 mg aliquots yielded 29 mg of material for RADA-16-I and 25 mg for RLDL-16-I that were characterized by analytical HPLC profile and MALDI TOF mass spectrum recorded on Ultraflex TOF/TOF (Bruker Daltonics): 1671.3 ([M+H]$^+$) for RADA-16-I and 2007.5 ([M+H]$^+$) for RLDL-16-I. The calculated MW values were 1672 for RADA-16-I and 2008 for RLDL-16-I.

Preparation of Peptide Solutions

Lyophilized proteins were dissolved in water at concentrations 1–3 mg ml^{-1} for RADA-16-I and 1 mg ml^{-1} for RLDL-16-I. This stock solution was sonicated in an ultrasonic bath (Pro's Kit) for 10 minutes and then centrifuged at 10,000 rpm for 10 min (Eppendorf minispin centrifuge) to remove insoluble aggregates, while the precipitate was discarded. The stock solution was stored at 4°C and diluted by water, 20 m*M* Hepes buffer (pH 7) or 10 m*M* HCl just before the measurements.

AFM Imaging

AFM samples were prepared on freshly cleaved mica by incubating a 10 µl drop of peptide solution for 2–5 min. Then the samples were washed two times with milliQ water and dried with a stream of nitrogen. AFM images were obtained using NTegra Prima microscope (NT-MDT, Russia) in semicontact (tapping) mode. Ultra sharp probes were used to achieve better special resolution.[23] Images were processed using Image Analysis (NT-MDT, Russia) and Femtoscan Online (Advanced technologies center) software.

Molecular Dynamics Simulations

Virtual models of RADA-16-I and RLDL-16-I peptide dimers, tetramers, and octamers were obtained by molecular docking of the corresponding 3D models[16] either with HEX v6.1 or GRAMM-X[24] software packages. Octamer energy was minimized and all-atom molecular dynamics simulations were carried out using the AMBER ff03 reaction force field[25] for 10 ns in explicit water. The resulting octamers were visualized with USCF Chimera.[26]

Thioflavin T Binding Assay

Thioflavin T (ThT) binding was measured with a Varian Cary Eclipse Fluorescence Spectrophotometer in a quartz 120 µl microcuvette. Stock solution of ThT (1 m*M*) was prepared in PBS. The solution for the measurements was prepared in a microcuvette by mixing ThT, peptide and PBS buffer to obtain 1–10 µ*M* ThT and up to ~0.15 mg ml^{-1} (90 µ*M*) peptide. The fluorescence (emission) spectra were recorded at 445 nm excitation.

NMR Spectroscopy

The samples for NMR were dissolved in D_2O/H_2O (100 µl D2O was added per 500 µl of 1 µg ml^{-1} aqueous sample solution for lock signal stabilization) at pH 7 and pH 2 (200 µl of 1*M* HCl was added to the pH 7 sample solution).

All NMR data were obtained with a Bruker AVANCE III 500 MHz spectrometer equipped with a Prodigy TCI cryogenic triple-resonance probe. The sample temperature was kept at 300 K during the NMR experiments. 1D proton and 2D NOESY spectra were measured for partial backbone resonance assignment (noesygpphw5 pulse sequence, relaxation time 1.2 s, and mixing time 50 ms). 2D DOSY spectra were measured to study the peptide aggregation (the stimulated echo pulse sequence with bipolar gradient pulses was used).[27] The water signal was suppressed by the WATERGATE pulse sequence with five pairs of symmetric gradients in all spectra (125 ms delay for binomial water suppression and 200 ms delay for gradient recovery).[28]

The NMR data processing and analysis were performed using Bruker TopSpin v.3.2, MATLAB 2014 (MathWorks, USA) (in-house scripts for phase correction and noise and residue water signal removing) and Sparky.

RESULTS AND DISCUSSION

Measurements of Fibril Size

Both studied peptides, RADA-16-I and RLDL-16-I, form nanofibers in the aqueous environment (Figures 1a and 1b). The fibrils observed after deposition from 20 m*M* Hepes buffer (pH 7) and from water (pH 5.5) were similar. The morphology of RADA-16-I fibrils has been examined by AFM previously.[9,12–14] The ability of RLDL-16-I to form similar fibrils is not surprising, since the peptides have similar alternation of hydrophobic and hydrophilic residues. RADA-16-I fibrils were typically longer than RLDL-16-I fibrils under the provided conditions.

We measured the fibril height above mica surface and obtained histograms with several peaks shown in Figures 1c and 1d. A certain repeating gap (1.8 nm for RADA-16-I and 2.4 nm for RLDL-16-I) between the peaks was observed, the gap value was interpreted as the bilayer thickness. Thus, the observed fibrils were interpreted as stacks of an even number of β-sheets (with hydrogen bonds oriented along the fibril axis). The fundamental element of these structures is a bilayer, rather than a monolayer. Bilayer formation is facilitated by the interaction of hydrophobic Ala and Leu residues for RADA-16-I and RLDL-16-I, respectively. This result agrees well with the observation that a bilayer protofibril is the minimal protofilament in amyloid fibrils.[29]

Many peptide and protein fibrils are twisted, which is believed to originate from amino acid chirality. Twisting was observed for amyloids (Aβ-peptide,[30] Gerstmann-Sträussler-Scheinker disease peptide[31]) and some amyloid-like fibrils (e.g. recombinant spidroin 1F9,[32] b-lactoglobulin[33]). We did not observe fibril twisting in RADA-16-I or RLDL-16-I samples, in agreement with the previous AFM observations of RADA-16-I fibrils.[13–15]

To quantify the observed difference between RADA-16-I and RLDL-16-I fibrils, we carried out molecular dynamics simulations. There are two molecular models proposed for the acetylated RADA-16-I fibrils with parallel[18,19] and antiparallel[13,15] β-sheets. We have obtained both parallel and antiparallel β-sheet dimers of the native RADA-16-I by molecular docking; however, the parallel β-sheet dimer was far less stable than the antiparallel one, according to the free energy values.

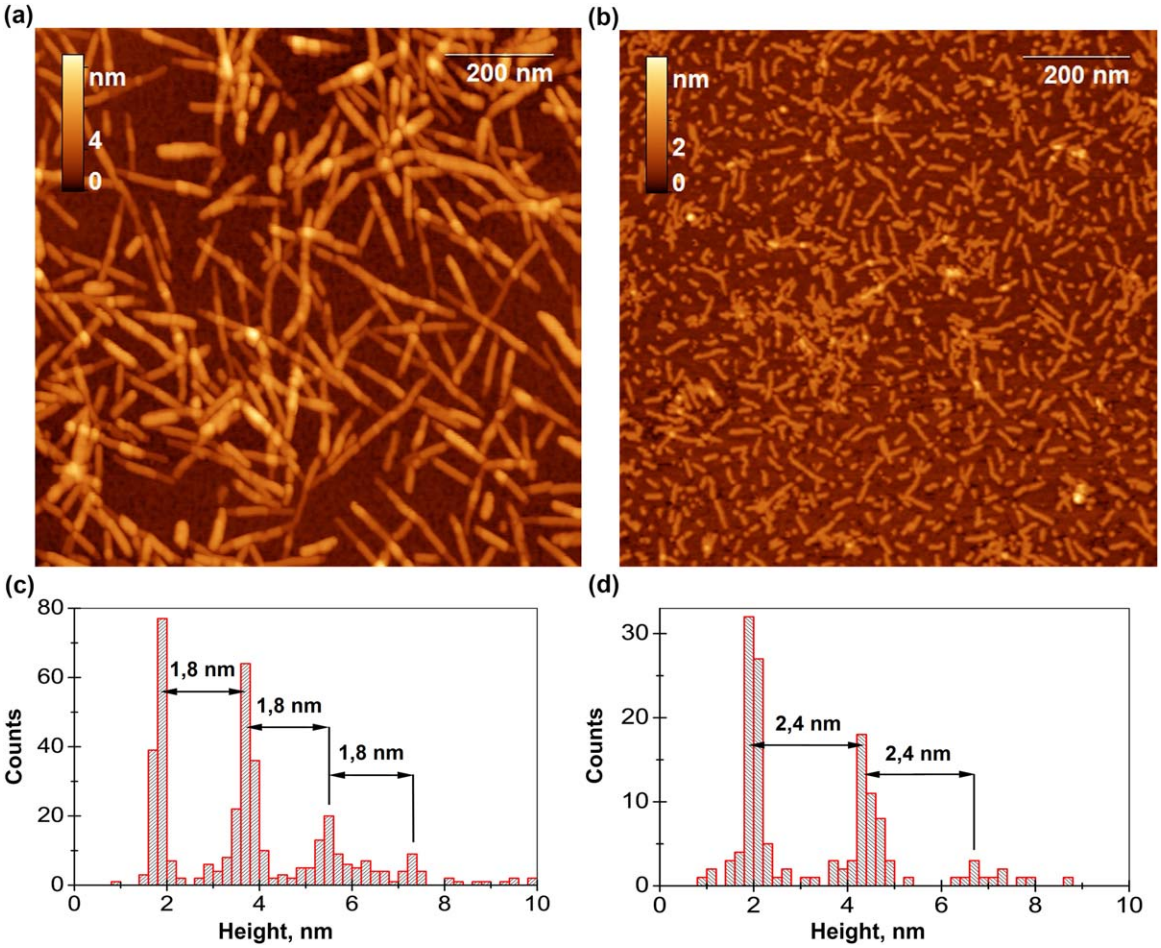

FIGURE 1 AFM images of RADA-16-I and RLDL-16-I fibrils. (a) AFM image of RADA-16-I fibrils deposited on mica, (b) AFM image of RLDL-16-I fibrils deposited on mica (c) Histogram of RADA-16-I fibrils height distribution showing 1.8 nm gap between the peaks, (d) histogram of RLDL-16-I fibrils height distribution showing 2.4 gap between the peaks.

This finding was confirmed during the MD simulation experiments in explicit water. The parallel β-sheet dimer of RADA-16-I was unstable and mainly dissociated into monomers; the relatively stable antiparallel β-sheet dimer retained the peptide association, although in a less structured conformation. Generally, the antiparallel β-sheet is the most stable supramolecular arrangement of a peptide dimer.[34] Because we study the peptide with the native N- and C- termini, the antiparallel β-sheet conformation was chosen to model the fibrils in the MD experiments.

During the molecular dynamics simulations a peptide octamer was chosen as a representative part of a bilayered fibril. The 3D models of RADA-16-I and RLDL-16-I octamers (Figure 2) after energy minimization had the same width (5.1 ± 0.12 nm) corresponding to the peptide chain length. Thickness of octamers was calculated as the mean distance between the opposite octamer surfaces limited by the Van der Waals radii. Thickness was 1.9 ± 0.1 nm and 2.3 ± 0.4 nm for RADA-16-I and RLDL-16-I, respectively. The excellent agreement of the AFM measurements and MD simulation data confirms that the peaks at the height histograms (Figures 1c and 1d) indeed correspond to the fibrils with different number of bilayers.

Thioflavin T Spectroscopy

Thioflavin T is a fluorescent dye that exhibits characteristic fluorescence upon binding to amyloid and amyloid-like fibrils.[35–37] We have shown that characteristic fluorescence appears when RADA-16-I fibrils are added to a cuvette containing ThT solution (Figure 3). ThT does not produce the characteristic fluorescent signal without the peptide; upon the addition of RADA fibrils, the fluorescence appears with the maximum at 482 nm. ThT fluorescence confirms that RADA-16-I fibrils possess a cross-β-sheet structure.

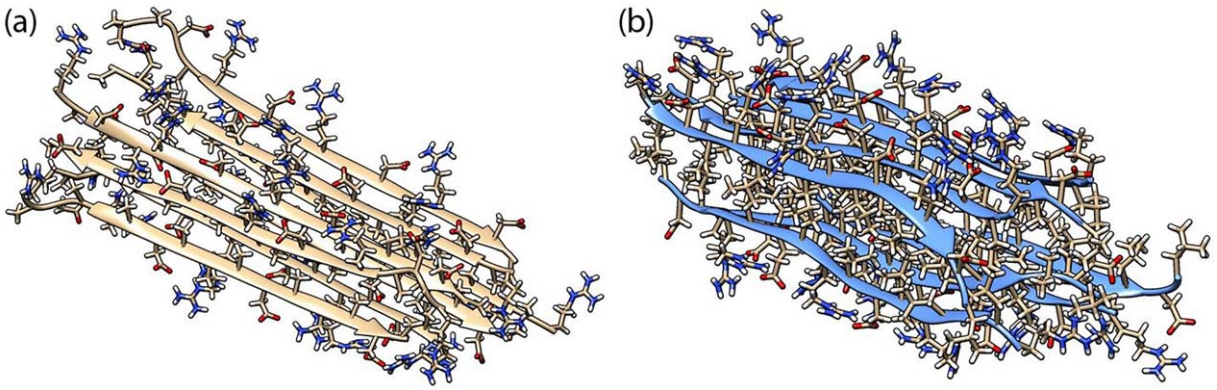

FIGURE 2 The 3D models of self-organized peptide octamers: RADA-16-I (a) and RLDL-16-I (b).

Rapid rotation around the central C—C bond prevents photon emission from the free ThT molecules.[38] Binding with a fibril hinders the torsional mobility of the central C—C bond and gives rise to fluorescence. ThT shows fluorescence upon binding to amyloid-like fibrils (e.g., spidersilk fibrils[39]) as well as to amyloids, thus there is no contradiction between the biodegradability of RADA-16-I scaffolds and the observed binding of RADA-16-I with ThT.

We could not observe the characteristic fluorescence from mixtures of RLDL-16-I and ThT. This may be explained by a lower dye binding constant or a lower peptide concentration (due to the lower RLDL-16-I solubility).

NMR Spectroscopy

RADA-16-I has three ion states: acidic (fully protonated), zwitterionic (electrically neutral, carrying partial positive and negative charges) and basic (fully deprotonated).[14] A significant pH change disrupts the fibril structure and increases the number of monomeric peptide molecules. The fraction of monomeric peptide at pH 2 is 60% ± 25%, as measured by size-exclusion chromatography (for the acetylated form of RADA-16-I).[15] We used low pH to disrupt the fibril structure; 2D DOSY experiment was chosen to compare the molecular weight of RADA-16-I aggregates in neutral (pH 7) and acidic (pH 2) medium. The results are shown in Table I. To estimate the molecular weight of the aggregates, we used the calibration curve described in the Supporting Information (Figure S1).[40]

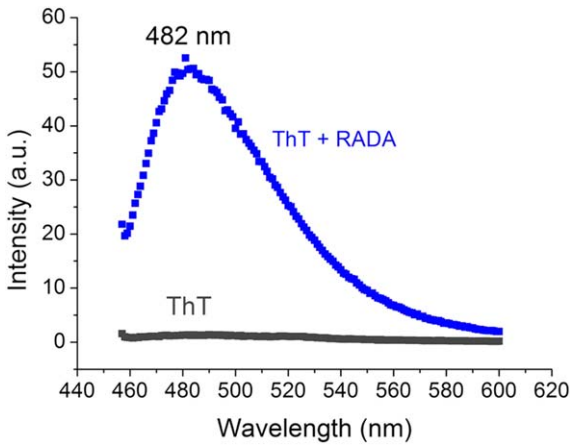

FIGURE 3 Fluorescence spectra of ThT (black) and ThT+RADA-16-I (blue) recorded at 445 nm excitation. The spectra were obtained at 11μM ThT and 0,1 mM RADA-16-I.

Two types of RADA-16-I aggregates were observed in both neutral and acidic media: the small ones, with the calculated molecular weight in the range of 3400–4500 Da, and the large ones, with the molecular weight of more than 39 kDa. The total amount of the aggregates did not change during the spectra acquisition. We interpret the small aggregates as mono- or dimers of RADA-16-I with different mobility in solution and the large aggregates as the RADA-16-I fibrils. Therefore, in neutral medium, RADA-16-I is mainly in the form of fibrils that are disrupted in acidic medium.

To prove the RADA-16-I fibrils disassembly under acid conditions, we acquired 1D proton NMR spectra with water signal suppression by WATERGATE and 2D NOESY spectra under neutral and acid conditions. The peaks in both spectra were partially assigned with the help of BMRB data bank.[41]

RADA-16-I samples contain a trace of impurities, particularly residual acetonitrile after HPLC purification. The comparison of RADA-16-I 1D NMR spectra in neutral and acidic media is shown in Figures 4 and 5. The main differences are the chemical shift and intensity changes of backbone amide protons peaks (Figure 5) and the chemical shift and coupling constant change of aspartic acid beta protons (Figure 4). The latter are diastereotopic in acidic medium, as in the free aspartic acid molecule, but magnetically equivalent in neutral medium. This difference may be caused by the hydrogen bonding of aspartic acid amide proton that results in the

Table I RADA-16-I DOSY Results

	Main Fraction		Trace fraction	
pH	Diffusion Coefficient (10^{-10} m^2 s^{-1})	Calculated Molecular Weight (Da)	Diffusion Coefficient (10^{-10} m^2 s^{-1})	Calculated Molecular Weight (Da)
2	2.7	3300	93	88,000
7	39	39,000	3.7	4500

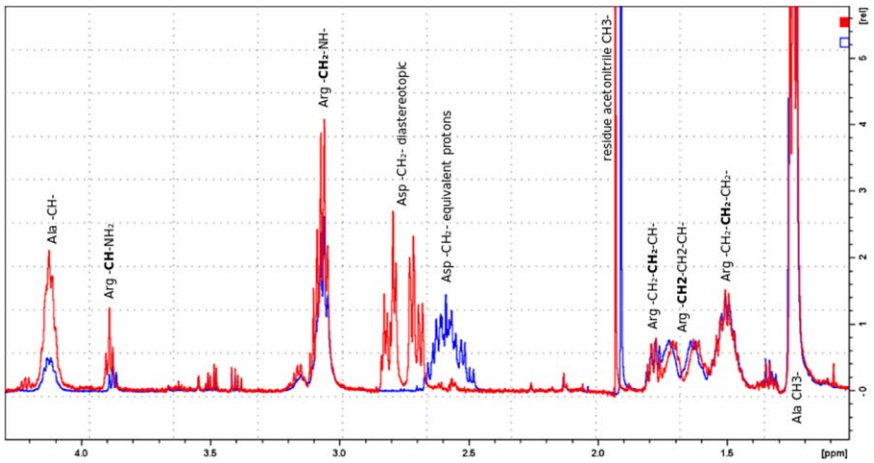

FIGURE 4 The 1D NMR 500 MHz WATERGATE spectra of RADA-16-I under acid (red) and neutral (blue) conditions, 1–4.3 ppm fragment. Assigned protons are shown in bold.

conformation change of RADA-16-I aspartic acid fragment. The changes of the amide proton intensities in neutral medium may be interpreted as the result of H-D exchange rate reduction caused by the hydrogen bonds in neutral medium.

To characterize the hydrogen bonds, we used 2D NOESY spectra (Figure 6). NOEs of three types of hydrogen bonds were found in the 2D spectra of RADA-16-I under neutral conditions: hydrogen bonds that involve backbone amide protons, hydrogen bonds between arginine and aspartic acid fragments, and hydrogen bonds between the arginine fragments. We could not clearly distinguish between the intermolecular and the intramolecular hydrogen bonds, this information can be obtained in future with the help of proton-carbon heteronuclear correlations NMR experiments.

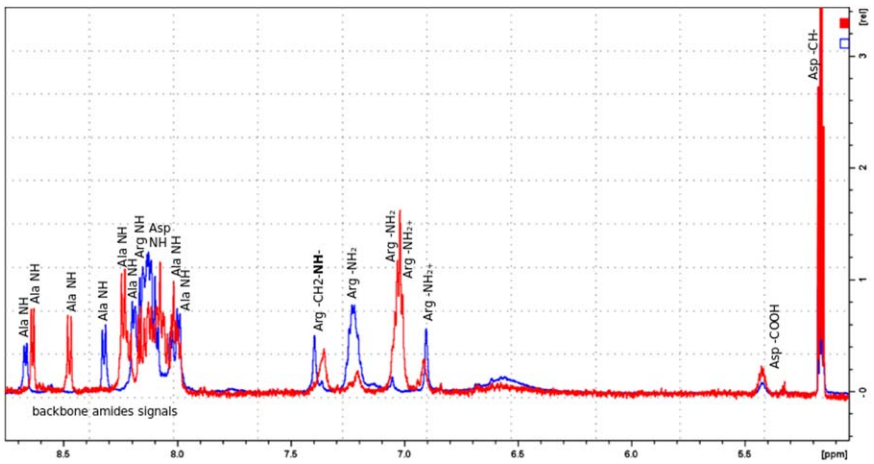

FIGURE 5 The 1D NMR 500 MHz WATERGATE spectra of RADA-16-I under acid (red) and neutral (blue) conditions, 5–8.7 ppm fragment. Assigned protons are shown in bold.

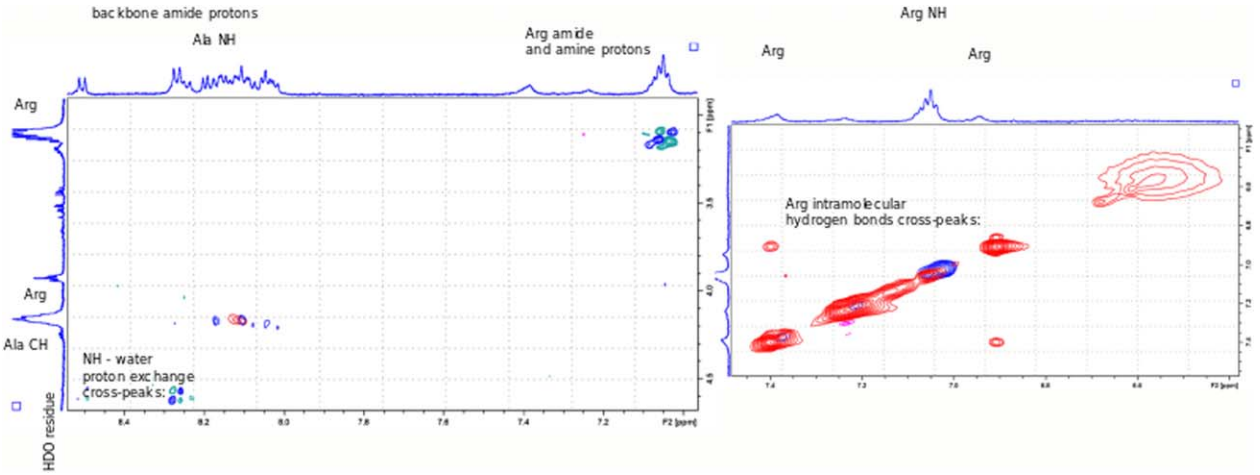

FIGURE 6 2D NOESY 500 MHz NMR spectra of RADA-16-I fragment (6.5–8.7 ppm) with hydrogen bonding NOEs. pH 7—red, pH 2—blue.

The crosspeaks of amide group protons with water were found in the NOESY spectrum of RADA-16-I in acidic medium. This fact is indicative of the existence of fast H-D exchange between the water protons and the amide group protons and can be interpreted as the absence of hydrogen bonds involving the amide group protons.

Thus, in acidic medium, the hydrogen bonds are absent between the RADA-16-I molecules backbones, as well as between aspartic acid and arginine fragments. This can be interpreted as the fibrils disassembly. The hydrogen bonds observed by NMR spectroscopy are in good agreement with the structural model described above (Figure 2).

Surface-induced Lamellae of RADA-16-I

Figure 7a shows an AFM image of RADA-16-I adsorbed on mica from a 1 μg ml^{-1} solution at pH 2. In acidic medium, we observed elongated structures of 0.7–1.1 nm in height. They can be interpreted as surface-induced lamellae (peptide monolayers). The observed height was consistent with the expected thickness of a monolayer 8.8–14.6 Å.[42] Similar peptide lamellae can be formed on mica from various peptides including Aβ(25–35),[43] GAV-9,[44] and P11-2.[45] Presumably, their structure is stabilized by the intermolecular hydrogen bonds between the adjacent peptide molecules, as in the β-sheets.

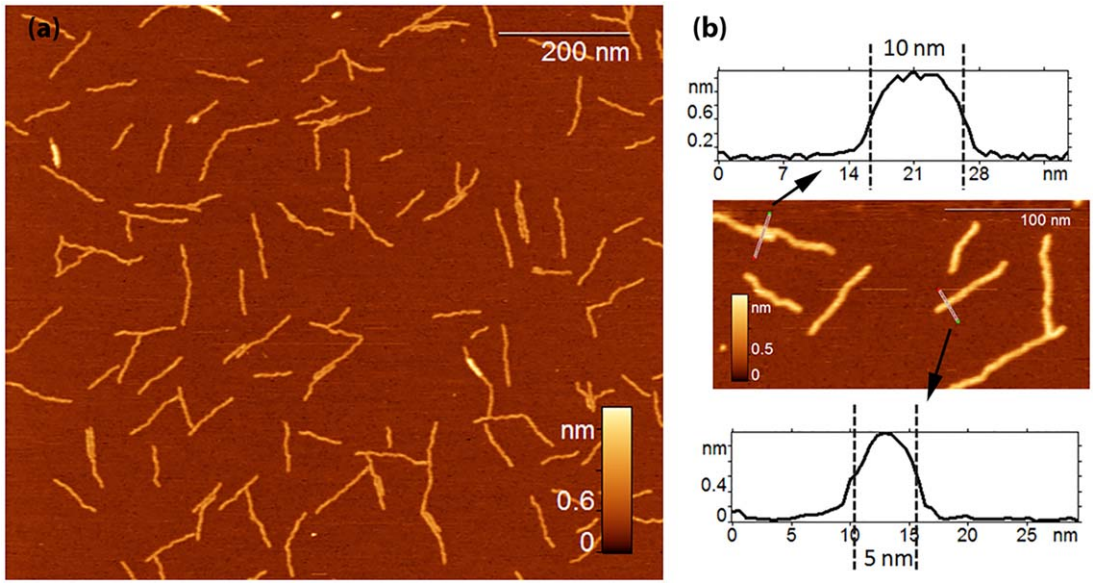

FIGURE 7 RADA-16-I monolayer sheets adsorbed on mica from acidic solution (a) typical scan, (b) sections. The sections are plotted along the lines crossing the two adjacent lamellae (top) and the single lamella (bottom).

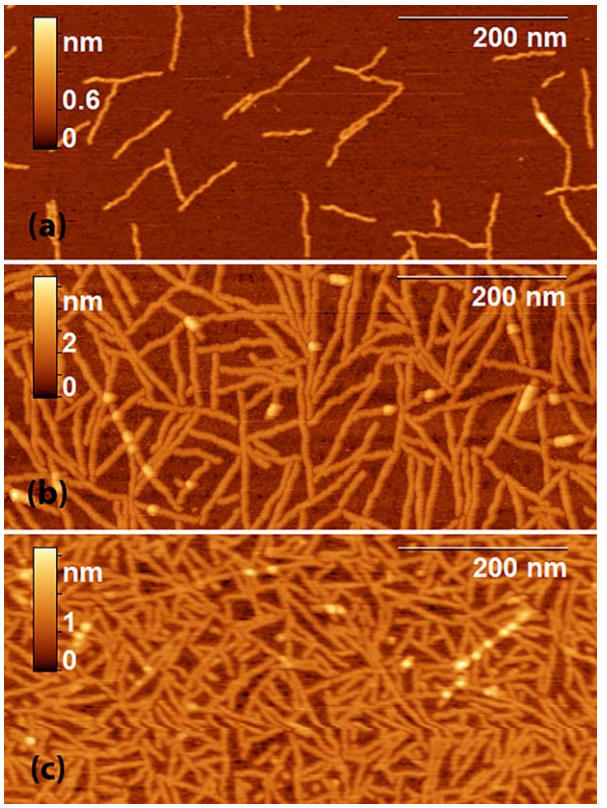

FIGURE 8 RADA-16-I adsorbed on mica from acidic solution at 1 μg ml^{-1} (a), 50 μg ml^{-1} (b), and 1 mg ml^{-1} (c).

We estimated the lamellae width as the peak width at half height (Figure 7b). Super-sharp cantilevers (∼1 nm radius) minimize the tip-broadening effect, so the measured width was not over-estimated, as in the case of common cantilevers (∼10 nm radius). The width of a single lamella was 5 nm, while for two lamellae adsorbed adjacent to each other it was 10 nm. These values are in perfect agreement with the peptide chain length of a single fully extended RADA-16-I molecule.

Some lamellae look undulating (winding), it can be explained by some imperfections of the molecular alignment. Presumably, during the lamellae formation, some molecules may slide along the backbone direction, decreasing the number of the hydrogen bonds between the adjacent molecules and giving rise to the undulations. Similar effects were observed in polyolefin lamellae on mica and HOPG.[46]

There is no evidence that structured RADA-16-I monolayers are unstable in solution, however they are stable on mica surface. This is one of the key findings of our study.

When the peptide concentration increased, the surface coverage increased as well (Figure 8). Although the second adsorbed layer of molecules could be formed, it appeared only as spare islands ∼1 nm above the first adsorbed layer even at high peptide concentration (∼1 mg ml^{-1}, Figure 8c). The layer-by-layer adsorption was hindered by the electrostatic repulsion between the first adsorbed layer and the molecules in solution.

Surprisingly, we were unable to observe the similar peptide lamellae on graphite. When RADA-16-I was deposited on graphite from acidic solution, it formed an amorphous layer (Figure 9a). The layer thickness was measured as the distance between two peaks on the histogram (Figure 9b), corresponding to the substrate and the peptide monolayer. The thickness was 1.4 nm, the difference in monolayer height on mica and graphite could be explained by the peptide-substrate interaction difference or peptide conformation difference.

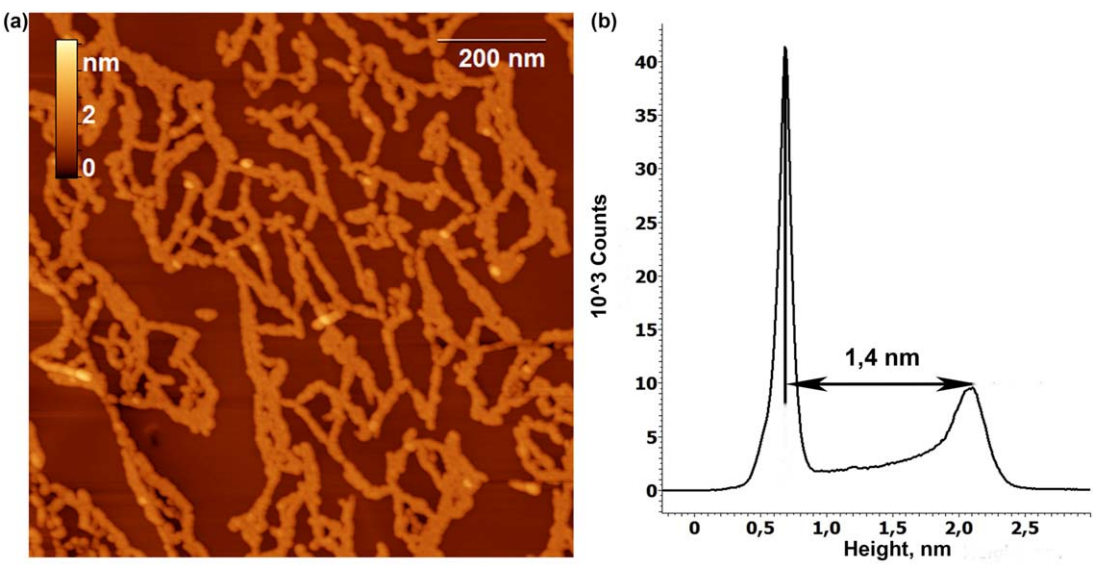

FIGURE 9 RADA-16-I adsorbed on graphite from acidic solution at 10 μg ml^{-1} (a), corresponding height histogram (b).

Graphite promotes the formation of epitaxial lamellae of many peptides including Aβ(1-42),[47] elastin-like peptides,[48,49] and EAK16-II.[50] Similar lamellae can be formed by hexaglycylamide.[51] The absence of epitaxial RADA-16-I monolayers on graphite is currently unclear. Probably, this is because of the strong electrostatic charge of the RADA-16-I molecules at pH 2 (low pH is necessary to prevent the molecules from aggregation into fibrils). It promotes the adsorption on the mica surface because of its negative charge. However, the interaction of RADA-16-I with graphite is presumably mediated by the relatively hydrophobic alanine residues, rather than electrostatic attraction. The uncompensated charge may prevent the lamellae formation.

The disassembly of RADA-16-I fibrils occurs in both acidic and alkaline media.[14] When RADA-16-I monomers adsorb on a substrate from acidic medium, they form monolayer lamellae on mica and an amorphous unstructured layer on graphite. We failed trying to obtain images of fibrils or lamellae of RADA-16-I deposited on a substrate from alkaline (10 m*M* KOH) medium. At high pH, we failed to observe RADA-16-I adsorbed on mica, graphite, GM-graphite (graphite functionalized by amino-groups[52]), mica coated with poly-L-lysine[53] and mica coated with 3-aminopropyltrietoxysilane (APTES) (data not shown). We explain this fact by the electrostatic repulsion between the peptide molecules and the substrate (e.g., mica) or by the damage of the NH_2 groups on the substrate (e.g., GM-graphite and mica coated with APTES).

CONCLUSION

RADA-16-I is a self-associating peptide forming the amyloid-like fibrils. Despite amyloid-like structure, RADA-16-I is known as biocompatible and biodegradable. RADA-16-I is usually obtained by solid state peptide synthesis and is used acetylated. To our knowledge, this is the first experimental study of deacetylated RADA-16-I.

We used AFM to compare RADA-16-I fibrils structure and morphology with the similar of RLDL-16-I peptide. The fibrils formed by both peptides were composed of stacked peptide bilayers, as many other amyloid fibrils.[29] The measured thickness of β-sheet bilayers (1.8 nm for RADA-16-I and 2.4 nm for RLDL-16-I) was confirmed *in silico* by the molecular dynamics simulations.

We have shown that RADA-16-I fibrils can bind with the ThT dye that is generally typical of amyloids. It can be used to monitor the RADA-16-I fibril growth kinetics. We failed trying to observe the binding of RLDL-16-I fibrils with ThT, probably due to the low RLDL-16-I solubility.

In the water-based environment, RADA-16-I is in either a monomeric or a fibrillar state. The transition between these states can be triggered by a change in pH. It was studied by NMR and observed as a change in RADA-16-I molecules diffusion and hydrogen bonding.

RADA-16-I adsorbed on mica from acidic medium formed monolayer lamellae of 1 nm in thickness (height). The lamellae width (5 nm) matched the peptide contour length indicating that the molecular backbone direction was perpendicular to the lamellar axis. The main difference between the lamellae and the fibrils is that the former are surface-induced and the latter are formed in the bulk. Mica surface properties are important for the formation of lamellae. RADA-16-I adsorbed on graphite from acid medium formed an amorphous layer of 1.4 nm in thickness.

Previously, the existence of monolayers of β-strands was hypothesized at the transient sticky ends of the growing RADA-16-I fibrils.[13] We have not found any experimental evidence supporting this hypothesis. We have shown that RADA-16-I monolayers can be artificially formed on mica under non-physiological conditions (in acidic medium). It is an important example of a surface-induced process for understanding of the molecular interactions between the RADA-16-I peptide and solid surfaces.

The authors thank Ms. Elizaveta Trifonova for proof-reading the manuscript.

REFERENCES

1. Westermark, P.; Benson, M. D.; Buxbaum, J. N.; Cohen, A. S.; Frangione, B.; Ikeda, S. I.; Masters, C. L.; Merlini, G.; Saraiva, M. J.; Sipe, J. D. Amyloid 2007, 14, 179–183.
2. Sipe, J.; Benson, M.; Buxbaum, J. Amyloid 2012, 19, 167–170.
3. Pulawski, W.; Ghoshdastider, U.; Andrisano, V.; Filipek, S. Appl Biochem Biotechnol 2012, 166, 1626–1643.
4. Fändrich, M. Cell Mol Life Sci 2007, 64, 2066–2078.
5. Bowerman, C. J.; Nilsson, B. L. Biopolymers 2012, 98, 169–184.
6. Zhang, S. Nat Biotechnol 2003, 21, 1171–1178.
7. Ellis-Behnke, R. G.; Liang, Y. X.; You, S. W.; Tay, D. K. C.; Zhang, S.; So, K. F.; Schneider, G. E. Proc Natl Acad Sci USA 2006, 103, 5054–5059.
8. Hsieh, P. C. H.; Davis, M. E.; Gannon, J.; MacGillivray, C.; Lee, R. T. J Clin Invest 2006, 116, 237–248.
9. Wang, T.; Zhong, X.; Wang, S.; Lv, F.; Zhao, X. Int J Mol Sci 2012, 13, 15279–15290.
10. Holmes, T. C.; de Lacalle, S.; Su, X.; Liu, G.; Rich, A.; Zhang, S. Proc Natl Acad Sci USA 2000, 97, 6728–6733.
11. Gelain, F.; Bottai, D.; Vescovi, A.; Zhang, S. PLoS One 2006, 1, 1–e119
12. Gelain, F.; Horii, A.; Zhang, S. Macromol Biosci 2007, 7, 544–551.
13. Yokoi, H.; Kinoshita, T.; Zhang, S. Proc Natl Acad Sci USA 2005, 102, 8414–8419.
14. Ye, Z.; Zhang, H.; Luo, H.; Wang, S.; Zhou, Q.; DU, X.; Tang, C.; Chen, L.; Liu, J.; Shi, Y. K.; Zhang, E. Y.; Ellis-Behnke, R.; Zhao, X. J Pept Sci 2008, 14, 152–162.

15. Arosio, P.; Owczarz, M.; Wu, H.; Butté, A.; Morbidelli, M. Biophys J 2012, 102, 1617–1626.
16. Danilkovich, A. V.; Sobolev, E. V.; Tikhonov, D. A.; Udovichenko, I. P.; Lipkin, V. M. Dokl Biochem Biophys 2012, 443, 96–99.
17. Aramvash, A.; Seyedkarimi, M. S. J Clust Sci 2015, 26, 631–643.
18. Cormier, A. R.; Lopez-Majada, J. M.; Alamo, R. G.; Paravastu, A. K. J Pept Sci 2013, 19, 477–484.
19. Cormier, A. R.; Pang, X.; Zimmerman, M. I.; Zhou, H. X.; Paravastu, A. K. ACS Nano 2013, 7, 7562–7572.
20. Rodionov, I.; Peshenko, I.; Baidakova, L.; Ivanov, V. Int J Pept Res Ther 2007, 13, 161–171.
21. Reid, G. E.; Simpson, R. J Anal Biochem 1992, 200, 301–309.
22. Kaiser, E.; Colescott, R. L.; Bossinger, C. D.; Cook, P. I. Anal Biochem 1970, 34, 595–598.
23. Klinov, D. V.; Lagutina, I. V.; Prokhorov, V. V.; Neretina, T.; Khil, P. P.; Lebedev, Y. B.; Cherny, D. I.; Demin, V. V.; Sverdlov, E. D. Nucleic Acids Res 1998, 26, 4603–4610.
24. Tovchigrechko, A.; Vakser, I. A. Nucleic Acids Res 2006, 34, W310–W314.
25. Case, D. A.; Cheatham, T. E.; Darden, T.; Gohlke, H.; Luo, R.; Merz, K. M.; Onufriev, A.; Simmerling, C.; Wang, B.; Woods, R. J. J Comput Chem 2005, 26, 1668–1688.
26. Pettersen, E. F.; Goddard, T. D.; Huang, C. C.; Couch, G. S.; Greenblatt, D. M.; Meng, E. C.; Ferrin, T. E. J Comput Chem 2004, 25, 1605–1612.
27. Johnson, C. S. Prog Nucl Magn Reson Spectrosc 1999, 34, 203–256.
28. Liu, M.; Mao, X.; Ye, C.; Huang, H.; Nicholson, J. K.; Lindon, J. C. J Magn Reson 1998, 132, 125–129.
29. Sawaya, M. R.; Sambashivan, S.; Nelson, R.; Ivanova, M. I.; Sievers, S. A.; Apostol, M. I.; Thompson, M. J.; Balbirnie, M.; Wiltzius, J. J. W.; McFarlane, H. T.; Madsen, A.; Riekel, C.; Eisenberg, D. Nature 2007, 447, 453–457.
30. Sachse, C.; Xu, C.; Wieligmann, K.; Diekmann, S.; Grigorieff, N.; Fändrich, M. J Mol Biol 2006, 362, 347–354.
31. Natalello, A.; Prokorov, V. V.; Tagliavini, F.; Morbin, M.; Forloni, G.; Beeg, M.; Manzoni, C.; Colombo, L.; Gobbi, M.; Salmona, M.; Doglia, S. M. J Mol Biol 2008, 381, 1349–1361.
32. Bogush, V.; Sokolova, O.; Davydova, L.; Klinov, D.; Sidoruk, K.; Esipova, N.; Neretina, T.; Orchanskyi, I.; Makeev, V.; Tumanyan, V.; Shaitan, K.; Debabov, V.; Kirpichnikov, M. J Neuroimmune Pharmacol 2009, 4, 17–27.
33. Adamcik, J.; Jung, J. M.; Flakowski, J.; De Los Rios, P.; Dietler, G.; Mezzenga, R. Nat Nano 2010, 5, 423–428.
34. Perczel, A.; Hudáky, P.; Pálfi, V. K. J Am Chem Soc 2007, 129, 14959–14965.
35. LeVine H, III. Methods Enzymol 1999, 309, 274–284.
36. Groenning, M. J Chem Biol 2010, 3, 1–18.
37. Sulatskaya, A. I.; Kuznetsova, I. M.; Turoverov, K. K. J Phys Chem B 2011, 115, 11519–11524.
38. Srivastava, A.; Singh, P. K.; Kumbhakar, M.; Mukherjee, T.; Chattopadyay, S.; Pal, H.; Nath, S. Chem Eur J 2010, 16, 9257–9263.
39. Slotta, U.; Hess, S.; Spiess, K.; Stromer, T.; Serpell, L.; Scheibel, T. Macromol Biosci 2007, 7, 183–188.
40. Li, W.; Chung, H.; Daeffler, C.; Johnson, J.; Grubbs, R. H. Macromolecules 2012, 45, 9595–9603.
41. Ulrich, E. L.; Akutsu, H.; Doreleijers, J. F.; Harano, Y.; Ioannidis, Y. E.; Lin, J.; Livny, M.; Mading, S.; Maziuk, D.; Miller, Z.; Nakatani, E.; Schulte, C. F.; Tolmie, D. E.; Kent Wenger, R.; Yao, H.; Markley, J. L. Nucleic Acids Res 2007, 36, D402–D408.
42. Fändrich, M.; Dobson, C. M. EMBO J 2002, 21, 5682–5690.
43. Karsai, Á.; Grama, L.; Murvai, Ü.; Soós, K.; Penke, B.; Kellermayer, M. S. Z. Nanotechnology 2007, 18, 345102.
44. Li, H.; Zhang, F.; Zhang, Y.; Ye, M.; Zhou, B.; Tang, Y. Z.; Yang, H. J.; Xie, M. Y.; Chen, S. F.; He, J. H.; Fang, H. P.; Hu, J. J Phys Chem B 2009, 113, 8795–8799.
45. Whitehouse, C.; Fang, J.; Aggeli, A.; Bell, M.; Brydson, R.; Fishwick, C. W. G.; Henderson, J. R.; Knobler, C. M.; Owens, R. W.; Thomson, N. H.; Smith, D. A.; Boden, N. Angew Chem 2005, 44, 1965–1968.
46. Prokhorov, V. V. In Structure and Properties of Polyolefin Materials; Nitta, K., Ed.; Kerala, India, Transworld Research Network 2012; pp 53–96.
47. Kowalewski, T.; Holtzman, D. M. Proc Natl Acad Sci USA 1999, 96, 3688–3693.
48. Yang, G.; Wong, M. K.; Lin, L. E.; Yip, C. M. Nanotechnology 2011, 22, 494018.
49. Yang, G.; Woodhouse, K. A.; Yip, C. M. J Am Chem Soc 2002, 124, 10648–10649.
50. Yang, H.; Fung, S. Y.; Pritzker, M.; Chen, P. PLoS One 2007, 2, e1325.
51. Prokhorov, V. V.; Klinov, D. V.; Chinarev, A. A.; Tuzikov, A. B.; Gorokhova, I. V.; Bovin, N. V. Langmuir 2011, 27, 5879–5890.
52. Adamcik, J.; Klinov, D.; Witz, G.; Sekatskii, S.; Dietler, G. FEBS Lett 2006, 580, 5671–5675.
53. Bussiek, M.; Mücke, N.; Langowski, J. Nucleic Acids Res 2003, 31, e137.